# SANDIA REPORT

SAND2020-9217
Printed August, 2020

Sandia National Laboratories

# Inverting infrasound data for the seismoacoustic source time functions and surface spall at the Source Physics Experiments Phase II: Dry Alluvium Geology

Christian Poppeliers, Leiph Preston

Prepared by
Sandia National Laboratories
Albuquerque, New Mexico 87185
Livermore, California 94550

Issued by Sandia National Laboratories, operated for the United States Department of Energy by National Technology & Engineering Solutions of Sandia, LLC.



Available to DOE and DOE contractors from

U.S. Department of Energy
Office of Scientific and Technical Information
P.O. Box 62
Oak Ridge, TN 37831

Telephone: (865) 576-8401
Facsimile: (865) 576-5728
E-Mail: reports@osti.gov
Online ordering: http://www.osti.gov/scitech

Available to the public from

U.S. Department of Commerce
National Technical Information Service
5301 Shawnee Road
Alexandria, VA 22312

Telephone: (800) 553-6847
Facsimile: (703) 605-6900
E-Mail: orders@ntis.gov
Online order: https://classic.ntis.gov/help/order-methods



# ABSTRACT

This report presents the infrasound data recorded as part of the Source Physics Experiment - Phase 2, Dry Alluvium Geology. This experiment, also known colloquially as DAG, consisted of four underground chemical explosions at the Nevada National Security Site. We focus our analysis on only the fourth explosion (DAG-4) as we determined that this was the only event that produced clear source-generated infrasound energy as recorded by the DAG sensors. We analyze the data using two inversion methods. The first method is designed to estimate the point-source seismoacoustic source time functions, and the second inversion method is designed to estimate the first-order characteristics (e.g. horizontal dimensions and maximum amplitude) of the actual spall surface. For both analysis methods, we are able to fit the data reasonably well, with various assumptions of the source model. The estimated seismoacoustic source appears to be a combination of a buried, isotropic explosion with a maximum amplitude of $\sim 2 \times 10^9$ Nm and a vertically oriented force, applied to the Earth's surface with a maximum amplitude of $\sim 4 \times 10^7$ N. We use the vertically oriented force to simulate surface spall. The estimated spall surface has an approximate radius of $\sim 40$ m with a maximum acceleration magnitude in the range of 0.8 to 1.5 m/s/s. These estimates are approximately similar to the measured surface acceleration at the site.

# ACKNOWLEDGMENT

The authors also acknowledge the National Nuclear Security Administration, Defense Nuclear Nonproliferation Research and Development (DNN R&D), and the Source Physics Experiment (SPE) working group, a multi-institutional and interdisciplinary group of scientists and engineers. Sandia National Laboratories is a multimission laboratory managed and operated by National Technology and Engineering Solutions of Sandia Limited Liability Corporation, a wholly owned subsidiary of Honeywell International, Inc., for the U.S. Department of Energy's National Nuclear Security Administration under Contract Number DE- NA0003525. This article describes objective technical results and analysis. Any subjective views or opinions that might be expressed in the article do not necessarily represent the views of the U.S. Department of Energy or the United States government.

# CONTENTS

# NOMENCLATURE

**Table 0-1.**

| Abbreviation | Definition |
|---|---|
| SPE | Source Physics Experiment |
| DAG | Dry alluvium geology |
| SGZ | surface ground zero |
| STF | source time function |
| RI | Rayleigh integral |

# 1. INTRODUCTION

The Source Physics Experiments (SPE) are a series of controlled, buried chemical explosions with the goal of understanding, among other things, the generation of so-called prompt signals from explosion sources. Some example of prompt signals are seismic waves, sound waves, and electromagnetic waves in the context of monitoring for explosion detection and discrimination (Snelson *et al*, 2013). To date, the SPE has completed two (of three proposed) phases, in which the first phase (SPE Phase I) consisted of a series of five chemical explosions detonated at various depths in granite (see Mellors *et al*, 2018 for details). The second phase of the SPE (SPE Phase II) consisted of a series of four buried chemical explosions detonated in dry, unconsolidated alluvium. The third phase of the SPE has not yet been conducted at the time of this writing.

The goal of this report is to describe our preliminary analysis of infrasound signals produced by the SPE Phase II series of explosions. This work follows, and to some extent is guided by, our previous analysis of SPE Phase I data, both infrasonic (Poppeliers *et al*, 2019; 2020) and seismic (Darrh *et al*, 2019). We proceed by describing the infrasound data and its characteristics. We then focus our analysis on estimating the physical attributes of the seismoacoustic source. We present two analysis methods, the first being a waveform inversion for the seismoacoustic source time function. Note that this first analysis method is similar to our analysis of the SPE Phase I infrasound data (e.g. Poppeliers *et al*, 2019; 2020). The second analysis is a waveform inversion as well, but the goal is to invert the data for a parametric model of the explosion-generated spall surface. The method is based on the Rayleigh integral, which was used by Jones *et al.* (2015) to model the infrasound recorded from the first two explosions of SPE Phase I.

We note that analysis contained herein is preliminary, and that this report serves mainly to document our current state-of-work. As this project matures, we will naturally refine our methods and interpretations, and hopefully integrate the various analysis techniques into a more complete understanding of the generation of infrasonic signals from this series of explosions.

## 1.1. EXPERIMENTAL SETUP

The SPE Phase 1 and Phase II were both conducted at the Nevada National Security Site (NNSS) during the years between 2011-2019. The chemical explosions of SPE Phase I were detonated in a single borehole, (albeit at different dates and depths) in the Climax Stock. Conversely, the explosions for the SPE Phase II, herein referred to as Dry Alluvium Geology, or DAG, were detonated in a single borehole that penetrated dry, porous, unconsolidated alluvium of Yucca Flat (Figure 1-1).

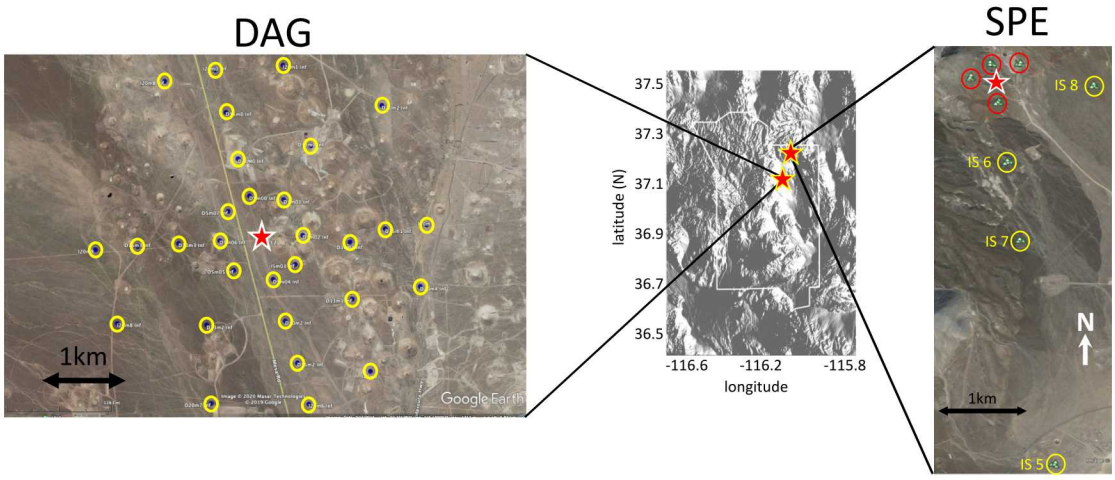


**Figure 1-1. Location of the SPE. To date, all SPE chemical explosions have been conducted at the Nevada National Security Site (NNSS) in Nevada, USA. (center panel) The SPE Phase I explosions were conducted in a single borehole in granite at the north end of NNSS (right panel). The DAG explosions were conducted in the dry alluvium of Yucca Flat a few tens of kilometers south of the SPE Phase I explosions. The panel on the left shows the layout of the infrasonic sensors that collected the data we analyze in this report.**

### 1.1.1. General Site Characteristics

The DAG tests where conducted in the broad sedimentary basin of Yucca Flat. Yucca Flat is a closed drainage basin formed as part of regional Basin and Range extensional tectonic activity. The floor of Yucca Flat slopes upwards towards the surrounding ranges in a series of coalescing alluvial fans that are composed of post-volcanic sedimentary fill that consists of a mixture of coarse-grained alluvial and colluvial deposits derived from the surrounding Cenonzoic silicic volcanic and Paleozoic siliciclastic and carbonate sedimentary rocks, playa deposits, and eolian sands. The alluvium in the vicinity of DAG is several hundreds of meters thick, and overlies bedrock (Sweetkind and Drake, 2007, Townsend et al, 2012). The sedimentary basin fill, which is several hundreds meters thick, lies unconformably on variably deformed pre-Cenozoic rocks and consist primarily of volcanic rocks such as welded and ash-fall tuffs.

### 1.1.2. The DAG chemical Explosions

The DAG series of four explosions were all conducted in the same borehole located at +37.11464423 latitude -116.0692643 longitude (Table 1). There were also a series of “cable

cutter" events, which were produced by literally cutting the tensioned cables after the explosive charge was emplaced. The cable-cutter events were too small to generate measurable infrasound and will not be discussed here. The DAG explosions were produced using nitromethane, contained in a sealed canister grouted in place within the borehole.

**Table 1-1. DAG explosions.**

| Experiment | Date | Origin UTC | Depth (m) | Yield (Metric Tons, TNT Equivalent) | SDO |
|---|---|---|---|---|---|
| DAG-1 | 20 July 2018 | 201:16:51:52.7 | 385.0 | 0.908 | |
| DAG-2 | 19 December 2018 | 353:18:45:56.9 | 299.8 | 51.0 | |
| DAG-3 | 27 April 2019 | 117:15:49:01.8 | 149.9 | 0.908 | |
| DAG-4 | 22 June 2019 | 173:21:06:19.9 | 51.6 | 10.357 | |

### 1.1.3. Raw Infrasound Data

The infrasound data (filtered to 0.1-100 Hz passband) is shown in Figure 1-2. Although there is a clear arrival of energy in the acoustograms for all four experiments, only DAG-4 shows clear evidence that this is acoustic energy generated at a point directly above the source. Specifically, the moveout velocity of the first arriving energy in DAG 1-3 shows that this energy is traveling too fast to be a source-generated acoustic arrival. Rather, this energy could either be energy arising from elastic-to-acoustic coupling at the Earth's free surface or seismic energy "leaking" onto the acoustic sensor due to imperfect ground isolation of the sensors. Regardless of the mechanism of the energy generating the signal on the acoustic sensor, a seismic-generated arrival will have a moveout velocity much greater than the horizontal acoustic wave speed due to the non-vertical incidence of the seismic wave field at the Earth's surface.

Our goal of this report is to analyze source-generated infrasound arising from the buried explosion. Based on the moveout velocities measured in Figure 1-2, only DAG-4 shows a clear source-generated infrasound arrival. Because of this, we will focus our analysis only on DAG-4. The analysis is in the far-field regime, with the simplifying assumptions of an approximate point source (or a source that's on the order of approximately one acoustic wavelength) and that the sensors are several wavelengths from the origin of the acoustic energy.

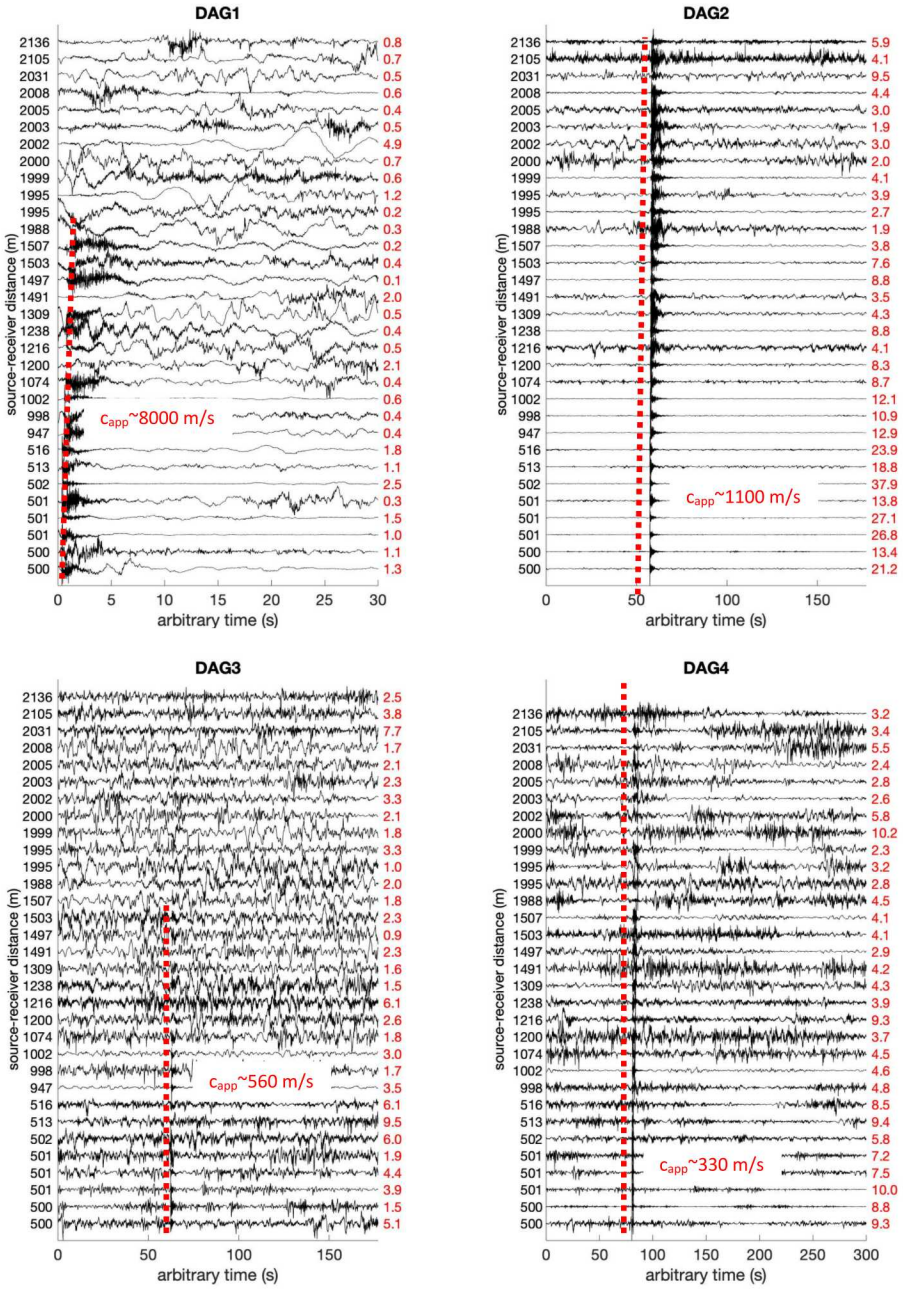


**Figure 1-2. Raw infrasound data for the four DAG experiments, filtered to 0.1-100 Hz passband. In each panel, the maximum acoustogram amplitude, in Pa, is given by the red numbers on the right side of the panel. The red dashed line is the approximate linear fit to the first arriving energy, slightly offset for display purposes. To the right of the dashed line is the apparent moveout velocity of the first arrival. In all cases but DAG-4, the first arriving energy has a wave speed consistent with a seismic arrival.**

# 2. ANALYSIS METHODS

We perform waveform inversions of the DAG-4 infrasound data using two different methodologies. The first method follows our previous work with the SPE Phase I, where we invert the data for seismoacoustic source time functions. The second method is based on the work of Jones *et al* (2015), where the goal is to invert the data for a parametric model of the spall surface. Note that this second inversion method is original, in that we developed it specifically for this data. It is based on the Rayleigh integral, which models acoustic energy radiation from a acceleration surface. For clarity of terminology, we will henceforth refer to the first inversion scheme as the STF-inversion and the second inversion as the RI-inversion.

## 2.1. METHOD 1, STF-INVERSION: ESTIMATING THE SEISMOACOUSTIC SOURCE TIME FUNCTION

A linear model predicting seismoacoustic waves $u$ at point $\mathbf{x}'$ in the far field is

$$u_k(\mathbf{x}',t') = \sum_{n=1}^{6} \int_{-\infty}^{\infty} g_{kn}(\mathbf{x}',t';\mathbf{x},t) m_n(\mathbf{x},t) dV dt \tag{2.1}$$

where $g_{kn}$ is the Green's function describing the impulse response from source $n$ located at $\mathbf{x}$ to receiver $k$ at $\mathbf{x}'$, and $m_n$ are a series of time varying force couple acting at point $\mathbf{x}$ in the Earth. In this model, the form of $m_n$ is arbitrary, but for pure earthquake sources takes the form of a symmetric, rank-2 tensor describing the relative contribution of each force couple on the total seismic source.

In our previous analysis, (Poppeliers *et al*, 2019) we assumed that the infrasound energy observed in the far field was a superposition of a buried, isotropic source and a vertically oriented force applied to the Earth's surface directly above the buried explosion. We take a similar approach here, where we assume that the data is a linear combination of an isotropic explosion source and a vertically oriented force at the Earth's surface. We also assume that both of these sources are time

variable and independent. In this case, equation 2.1 becomes

$$\begin{aligned} u(\mathbf{x}',t) &= \sum_{i=1}^{2} \left( G^{(i)}(\mathbf{x}';\mathbf{x}_i,t) \otimes m^{(i)}(\mathbf{x}_i,t) \right) \\ &= \left( G^{(1)}_{expl}(\mathbf{x}';\mathbf{x}_1,t) \otimes \mathbf{M}_{expl}(\mathbf{x}_1,t) \right) + \left( G^{(2)}_{F}(\mathbf{x}';\mathbf{x}_2,t) \otimes \mathbf{F}(\mathbf{x}_2,t) \right) \\ &= G^{(1)}_{expl}(\mathbf{x}';\mathbf{x}_1,t) \otimes \begin{bmatrix} M_{xx} & 0 & 0 \\ 0 & M_{yy} & \\ 0 & 0 & M_{zz} \end{bmatrix} + G^{(2)}_{F_z}(\mathbf{x}';\mathbf{x}_2,t) \otimes \begin{bmatrix} 0 \\ 0 \\ F_z \end{bmatrix} \end{aligned} \tag{2.2}$$

in which $\otimes$ denotes time domain convolution, $G^{(1)}_{expl}$ and $G^{(2)}_{Fz}$ are the pressure Green's functions from an explosion source located at $\mathbf{x}_1$ and the vertical force source located at $\mathbf{x}_2$, respectively, to the receiver $k$ located at $\mathbf{x}$ for a time-domain moment tensor $\mathbf{M}_{expl}$ and a surface-located time dependent force $\mathbf{F}_z$, respectively. In this model, we explicitly assume that the buried explosion source $\mathbf{M}_{expl}$ is a buried isotropic explosion and thus $M_{xx} = M_{yy} = M_{zz}$. Note also that the vertical force source term $\mathbf{F}_z$ is assumed to be purely vertical, and is an approximation of surface spall.

Rewriting equation 2.2 in the frequency domain yields

$$u(f) = \sum_{i=1}^{2} G^{(i)}(f) S^{(i)}(f) \tag{2.3}$$

where $S^{(1)} = \mathbf{M}_{expl}(f)$ and $S^{(2)} = \mathbf{F}_z(f)$ are the spectra of the source terms. In matrix form, equation 2.3 is written as:

$$\mathbf{u} = \mathbf{G}\mathbf{m}. \tag{2.4}$$

where $\mathbf{u}$ is the frequency domain data, $\mathbf{G}$ is a model, or predictor, matrix containing the frequency domain GFs, and $\mathbf{m}$ is a vector containing the STFs of the moment tensor (see equations 6-8 of Poppeliers *et al.*, 2019 for details).

The most computational demanding part of inverting the data using the scheme presented in this section is the estimation of the Green's functions. For this work we estimated the Green's functions similarly to those estimated in our analysis of the SPE Phase I data, so we will only summarize the process here. The major difference between the Green's functions that we used in our previous SPE Phase I analysis and those estimated here is that we use a fully elastic model, whereas in the SPE Phase I analysis, we used a fully acoustic model. We constructed our three-dimensional elastic model with two regions, one simulating the Earth and one simulating the air. The model had physical dimensions of 4100 x 3900 x 1070 meters, with a discrete grid node spacing of 2.5 m. The wave speeds in the Earth portion contained non-zero values for both the compression and shear wave, and are based on the Yucca Flat Geologic Framework Model (Prothro *et al.*, 2016). To simulate the acoustic portion of the model, we set the compressional wave speed to a value typical of air ($\sim$ 340 m/s) and the shear wave speed equal to approximately zero (specfically, $10^{-6}$ m/s). Then we estimated the Green's functions for the explosion source by using a finite difference solution to the three dimensional elastic wave equation where the initial conditions simulate the necessary seismic sources. For example, to simulate the explosion-source

Green's functions, the initial condition is simulated by placing a unit amplitude delta function, with an isotropic moment tensor, in the model so that its position relative to the recording receivers matches that of the actual experiment (Figure 1-1). To estimate the Green's function of the vertically oriented force, the initial condition consisted of a delta function source time function, directed upwards at the earth/air interface, where its horizontal position coincided to surface ground zero (SGZ). For all of the finite difference simulations, the discrete time step was $1.484 \times 10^{-4}$ seconds. We ran the finite difference simulation for 17.0 seconds of model time, and collected the pressure wavefield at locations corresponding to those of the DAG infrasound receivers.

## 2.2. METHOD 2, RI-INVERSION: PARAMETRIC INVERSION FOR AN EQUIVALENT SPALL SURFACE

For this method, we make simplifying assumptions about the source model of the infrasonic wavefield. Specifically, we assume that the infrasound is produced solely by a finite-area surface, with a time variable acceleration history. We also assume that this surface, which simulates spall, can be approximated with simple functional forms, such as two-dimensional Gaussian surfaces, or a piston. This parametric inversion approach attempts to fit the data with very simple source models, which are parameterized by only a few variables. The point of this approach is to very quickly estimate, to the first order, the surface deformation that caused the observed infrasound. The hope is that when the surface deformation is estimated, this surface can be used to estimate the yield of the buried explosion.

Our forward model predicts the data using the Rayleigh integral where the observed time variable acoustic wavefield observed at station $k$ located at $\mathbf{x}$ is given as

$$u_k(\mathbf{x},t) = \frac{\rho_0}{2\pi R} \int\int_S a_s \left( \mathbf{x}', t - \frac{R}{c_0} \right) dS \tag{2.5}$$

where $\rho_0$ is the air density, $c_0$ is the sound speed, $t$ is time, and $R$ is the distance between the observation point $\mathbf{x}$ and the surface point $\mathbf{x}'$ on the function $a_s$. The term $a_s$ is an arbitrarily shaped surface which defines the vertical acceleration of the ground surface. The surface $a_s$ has an acceleration time history and the double integral indicates that it's summed over its area $S$ (e.g. Bannister, 1979; Kirkup, 1994; Jones *et al.*, 2015).

We can approximate the surface acceleration $a_s$ with any number of two-dimensional functions. However, for our work here we use a two-dimensional Gaussian surface and a rigid piston. The Gaussian surface has form

$$a_s(x',y',t) = \frac{A(t)}{2\pi} \exp\left[ -\left( \frac{(x'-x)^2}{(2\sigma_x)^2} + \frac{(y'-y)^2}{(2\sigma_y)^2} \right) \right] \tag{2.6}$$

where $x'$ and $y'$ are the local coordinates of the surface and $\sigma_x$ and $\sigma_y$ describe the effective width in the cardinal directions (Figure 2-1). This first parameterized model of the spall surface was

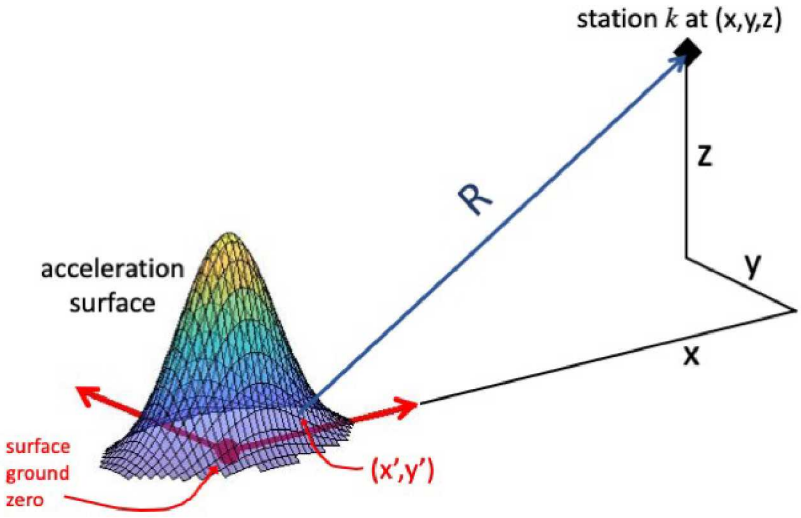


**Figure 2-1. Definition of the model space. The observation point at station $k$ is located at $(x,y,z)$, where $R$ is the slant distance from the surface point $(x',y')$. In this case both coordinate systems has their origin at surface ground zero, and the acceleration surface is centered over SGZ. The surface $a_s(x',y')$ shown here is parameterized by $\sigma_x$ and $\sigma_y$, which describe the width of the Gaussian function (equation 2.6) in the $x$ and $y$ directions, respectively, and the amplitude. Note that this figure shows the spall surface for a single instant in time: the amplitude of the surface is actual a time-varying function described by $A(t)$.**

chosen as it closely resembles the observed surface accelerations seen in the SPE Phase I tests (Jones *et al*, 2015). This model is parameterized by only three terms: two that describe the spatial form of the surface and the time variable acceleration history $A(t)$ which we assume is similar over the entire surface.

A second surface acceleration model we consider is that of a simply piston. This is given by

$$a_s(r',t) = \begin{cases} A(t) & \text{if } r \le r_0, \\ 0 & \text{if } r > r_0 \end{cases} \tag{2.7}$$

where $r$ is the radial distance from the SGZ and $r_0$ is the total radius of the surface. We decided to add this parametric model to this inversion, as there was observational evidence that the spall surface took this form during the second DAG explosion.

Modeling the acoustic signal generated from these types of surfaces shows the signal is sensitive to the physical dimensions of the spall surface, its aspect ratio, as well as the frequency content of the acceleration function $A(t)$ (Fig. 2-2). In general, increasing the maximum acceleration amplitude will increase the amplitude of the observed infrasound. Furthermore, for a given time history $A(t)$, decreasing the center frequency of $A(t)$ will also result in an increasing amplitude of

infrasound. Finally, the radiation pattern of the infrasound is more pronounced at higher frequencies of $A(t)$ for both types of surfaces.

To form an inversion scheme, we minimize the L2 norm of the difference between the predicted data and the observed data:

$$min||u_{pred}(t) - u_{obs}(t)||^2 \tag{2.8}$$

where the data is predicted according to equation 2.5. To implement the inversion, we assume an acceleration time history (ideally chosen to match the observed data: see next paragraph), and grid search over the amplitude of the acceleration time history and the dimensional parameters of the assumed spall surface model.

By design, the inversion uses a first-order approximation of the spall surface acceleration that's parameterized by its physical dimensions and time-varying amplitude. Implicit in the model is the form of the spall surface time history $A(t)$, which can take any arbitrary form. However, the choice of $A(t)$ should be such that the waveform shape of the predicted data approximates that of the observed data, which we approach in a trial-and-error fashion. For the work we do here we begin by choosing $A(t)$ to be a first derivative Gaussian with a frequency content similar to that of the data. The primary reason for our choice of $A(t)$ is this function's waveform similarity to the observed data. One could, in principle, use the data itself to approximate a non-analytical function for $A(t)$, but we found that doing so only increased the complexity of the inversion approach without improving the misfit.

An additional parameter to consider is that of the presumed wavespeed. By choosing the acoustic wavespeed to be less than the wavespeed at the time of the data observation, the predicted data will contain acoustic arrivals that are delayed in time relative to those of the observed data. Conversely, by overestimating the acoustic wavespeed, the predicted acoustic energy will arrive too early. We address this by computing the best average acoustic wavespeed that minimizes the acoustic arrival time misfit between the observed data and the predicted data. Specifically, knowing the location and time of the buried explosion and the location of the acoustic sensors, we can compute the wavespeed between SGZ and the individual stations. We then average these computed wavespeeds and use this average as the wavespeed for the forward model.

An important assumption implicit in this formulation is that the observed infrasound wavefield is in the 'far-field'. The far-field is defined as the region where the source-receiver distance is greater than the Rayleigh distance, defined as

$$R_0 = \frac{S}{\lambda} \tag{2.9}$$

where $S$ is the area of the acoustic baffle and $\lambda$ is the wavelength of the signal. If we limit the analysis to frequencies less than 5 Hz, the maximum Rayleigh distance for a spall surface that's 200 m on a side is approximately 600 m. Note that as the size of the spall surface decreases, the Rayleigh distance decreases. Similarly, as the frequency of analysis decreases, the Rayleigh distance decreases. Based on the maximum frequency that we evaluate and field measurements of the spall surface, all of our infrasound sensors are well outside the Rayleigh distance, ensuring that the data is in the far-field propagation regime.

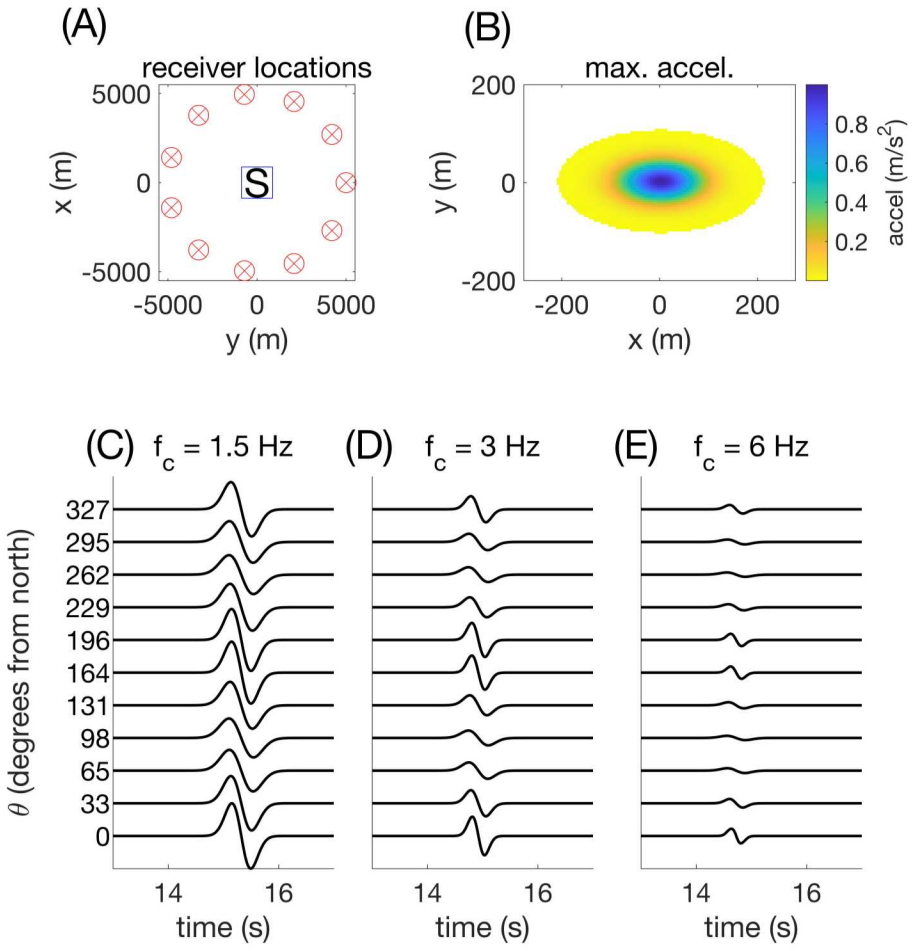


**Figure 2-2. An example of modeled infrasound using a two dimensional Gaussian acceleration surface. Panel (A) shows the geometry of the surface mounted (z=0 m) infrasound receivers. Panel (B) shows a snapshot of the acceleration surface at a time corresponding to its maximum amplitude, with physical dimensions of $\sigma_x$=20 m and $\sigma_y$=40 m. The modeled infrasound shown in the bottom panels were created using an acceleration time history $A(t)$ simulated by a first-derivative Gaussian with unit amplitude, with a center frequency of 1.5 Hz (C), 3.0 Hz (D), and 6.0 Hz (E). The acoustograms are arranged by the azimuth from north between the source and the receiver location and are scaled to the amplitude of the time series given using the 1.5 Hz acceleration time history recorded at the source-receiver azimuth of zero degrees.**

# 3. ANALYSIS AND RESULTS

Here we describe our analysis methods and the results of inverting the DAG-4 infrasound data. We do not invert the infrasound data from the first three DAG experiments, as there was no clearly identifiable source-generated acoustic signal observed. Rather, the signal seen on the acoustic sensors in these first three experiments was almost certainly seismic energy "leaking" into the acoustic sensors. Whether this is true elastic-to-acoustic energy, or simply the acoustic sensors not being adequately isolated from ground motion is unknown. Regardless, our goal here is to analyze source-generated infrasound energy, and thus we only focus our efforts on DAG-4.

Recall the STF-inversion inverts the data for an estimate of the seismoacoustic source time function and the RI-inversion attempts to estimate the dimensions of a simple spall model. Although these two phenomena are undoubtably linked, at this point, we treat them separately and analyze the data through the lens of each inverse method separately. Future work will focus on combining these two phenomena into a single unified physical model.

## 3.1. STF-INVERSION FOR SOURCE TIME FUNCTIONS

The forward model given in equation 2.1 allows for a completely generalized seismoacoustic source, albeit linear and a point source. However our previous work inverting the SPE-Phase 1 data showed that we can reduce the source model to contain only an isotropic explosion term and a vertically oriented, time variable force term applied at the surface directly above the buried explosion.

The preprocessing of the data prior to the inversion consisted of applying a 1-6 Hz passband filter and a pre-event mute. The mute was designed only to reject data that we judged not not be associated with the source event. Specifically, we visually inspected each acoustogram, and identified the direct acoustic arrival. We then started the mute 0.5 to 1 seconds prior to this direct acoustic arrival, depending on the source-receiver distance. All post-arrival energy was retained. Note that this muting strategy allowed near-receiver seismic-to-acoustic energy to be retained. Because our forward model (i.e. the Green's functions) accounted for this energy, we deemed it beneficial for the inversion.

Figures 3.1 - 3.3 show the results of inverting the data where the assumed source model was an explosion only, a vertical force only, and both an explosion and a vertical force, respectively. In all cases, we filter the estimated source time functions, data, and fit-to-data to 1-6 Hz passband. To help determine the fit-to-data for each presumed source model, we convolve the estimated source time functions with the Greens functions used for the inversion, which we will refer to the

predicted data $u_{pred}$. We then plot the predicted data on top of the observed data for visual inspection (Figures 3-1 through 3-3). Note that for all three source models, we generally fit the data, with minor variations in the phase of the predicted data. To quantify the misfit, or data residual, we can compute the data residual $R$ as the L2 norm of the absolute difference between the predicted data and the observed data

$$R = \sqrt{\sum_{i=1}^{N} |u_{pred}^{\{i\}} - u_{obs}^{\{i\}}|^2}. \tag{3.1}$$

Note that lower values of the data residual indicate a better fit. We can also quantify the misfit with a slightly more intuitive calculation, where we simply compute the correlation coefficients between the observed data and the predicted data. For this measure, higher values of the correlation coefficient suggest a better fit to data, as the correlation coefficient is a measure of waveform similarity here. The main caveat with using the correlation coefficient as a measure goodness of fit is that the correlation coefficient, as applied to waveform similarity, does not take into account the relative waveform amplitudes. In other words, given two waveforms with a correlation coefficient of $X$, changing only the amplitude of one of the waveforms will result in a correlation coefficient of $X$. So the correlation coefficient is more a measure of waveform similarity with respect to waveform phase, without regard to waveform amplitude. Note that we present the correlation coefficient for each acoustogram as well as the mean correlation coefficient in Figures 3.1 - 3.3.

Table 3.1 summarizes the results for the three different source models. Note that the source model that contains only the vertical force term $F_z$ has the lowest data residual (and corresponding highest mean correlation coefficient). Conversely, when the source model contained only an isotropic explosion term, the data fit was the worst. Using both source terms results in a data fit between these two end members. It's difficult to determine which source model is closest to reality. An important result, however, is that regardless of the source model used, the absolute maximum magnitudes of the relative source time functions is relatively similar. For example, the maximum absolute magnitude for the $F_z$ term is $4 \times 10^4$ N for the $F_z$-only model and the explosion + $F_z$ model. Likewise for the absolute magnitude of the explosion source time function. This suggests that the forward model captures the physics of the dual-source model quite well, and thus we weakly favor the two-source model here. We make this interpretation for two reasons: 1) the relative stability of all the estimated source time functions, regardless of the source model used, and 2) the relative similarity of the maximum amplitudes of the source time functions, regardless of the source assumptions.

## 3.2. RI-INVERSION FOR SURFACE ACCELERATION

For this analysis, the goal of the inversion is to estimate the size and time amplitude of a finite area surface that approximates the spall. We formulated our inversion so that we have the freedom to choose the acceleration time history as well as the functional form of the approximated spall surface. Then to fit the data, the inversion simply performs a grid search over a range of relavant size and maximum acceleration parameters.

**Table 3-1. Summary results for STF-inversion. The data were inverted using three different source model combinations, where we computed the mean correlation coefficient, data residual, and the absolute value of the maximum amplitude of the estimated source time functions corresponding to the assumed source model.**

| source type | mean correlation coefficient | data residual | maximum amplitude of estimated source |
|---|---|---|---|
| explosion | 0.6339 | 129.43 | 5 x $10^9$ J |
| $F_z$ | 0.7535 | 73.1 | 4 x $10^7$ N |
| explosion + $F_z$ | 0.7164 | 77.9 | explosion: 2.1 x $10^9$ J |
| | | | $F_z$: 4 x $10^7$ N |

Prior to inverting the data, we first apply a 1-6 Hz passband filter to all of the acoustograms. We then mute each acoustograms such that only direct, source-generated energy is present. We construct the mutes individually for each trace by first calculating the theoretical arrival time of the direct acoustic arrival. We then manually pick the actual arrival time of the direct acoustic energy, using the theoretical arrival time as a guide. We then construct a 1.3 second long Tukey window (25% taper at both ends) and apply it to the data at the computed arrival time. The window is designed to retain only the energy within the window, and thus rejects all other signal. Note that the mute strategy is more restrictive than that implemented for the STF-inversion. This is due to the fact that the forward model used for the surface acceleration inversion is based on the Rayleigh integral, which only models acoustic energy generated at the source. Thus any near-receiver seismic-to-acoustic energy will not be accounted for in our forward model and must be eliminated prior to inversion.

For our tests here, we tested two surfaces: a two dimensional Gaussian surface and a piston surface. For the acceleration time history, we used a first derivative Gaussian with a passband of 1-6 Hz. This time history was chosen in a rather trial-and-error method, and resulted in the best fit to data. In the case where the surface was assumed to be a Gaussian surface, we allowed the width parameters $\sigma_x$ and $\sigma_y$ to vary independently. The only width parameter for the piston model was the radius $r_0$ of the piston.

For both model types, the inversion fit the data approximately equally well (Table 3.2), based on the mean correlation coefficient and data residual. However, the maximum acceleration of the Gaussian surface model needed to be almost twice that of the piston surface model. To understand why, we plot the cross sections of the estimated maximum acceleration surface for both models, at the $y = 0$ line (Figure 3.6). Although the estimated Gaussian surface is taller than the piston surface, it is also not as wide, on average, as the piston. Narrower surfaces produce lower amplitude infrasound (see Figure 2-2), and thus the more narrow Gaussian surface must be of higher amplitude than the fatter piston surface in order to fit the data. Interestingly, the volume under each estimated acceleration surface is approximately equal ($Vol_{gaus} = 2.97 \times 10^3$ m$^3$, $Vol_{pist} = 2.69 \times 10^3$ m$^3$). This suggests that the total volume under the acceleration surfaces is a

**Table 3-2. summary results for inverting for the surface acceleration surface**

| surface model | size parameter | mean correlation coefficent | data residual | max$(A(t))$ |
|---|---|---|---|---|
| Gaussian | $\sigma_x = 12$ m<br>$\sigma_y = 12$ m | 0.779 | 60.24 | 1.5 m/sec$^2$ |
| piston | r = 30 m | 0.784 | 60.03 | 0.8 m/sec$^2$ |

more important parameter than their presumed functional form.

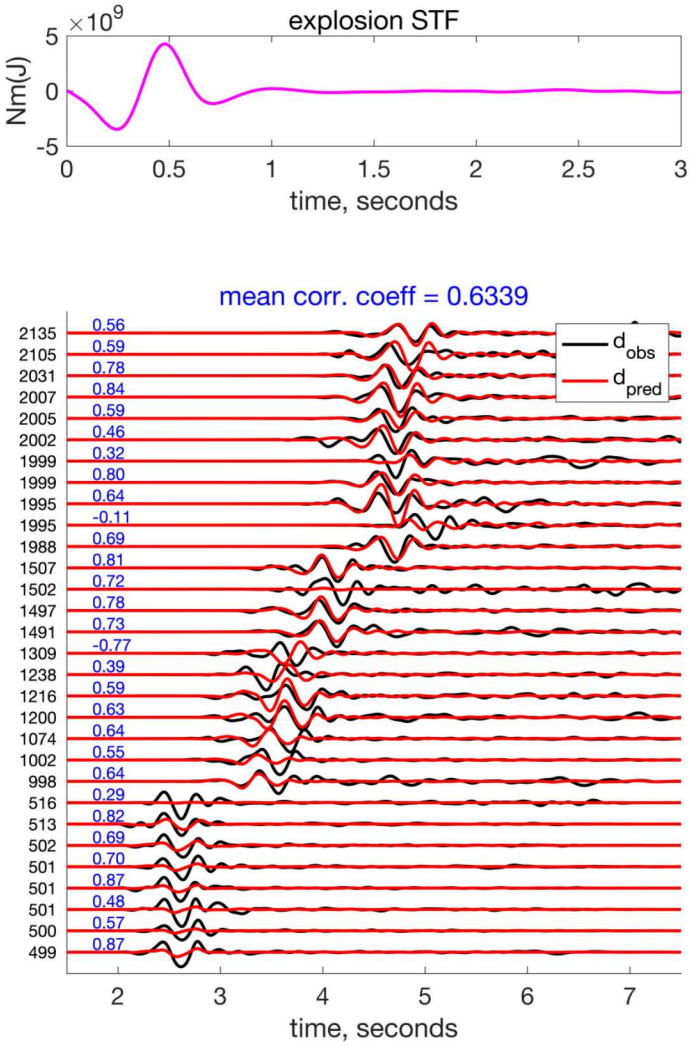


**Figure 3-1. Results of inverting the infrasound data for the equivalent source time function. For this result, the assumed source model was a buried, isotropic explosion. The top panel shows the estimated source time function and the bottom panel shows the observed data (black) and the predicted data (red). The blue numbers above each acoustogram (at approximately $t = 2$ s) is the correlation coefficient for each station. The black numbers along the y-axis are the distance, in meters, between the recording station and SGZ. Each pair of acoustograms are normalized to the maximum amplitude of the the observed data. The mean of all the correlation coefficients is shown at the top of this panel.**

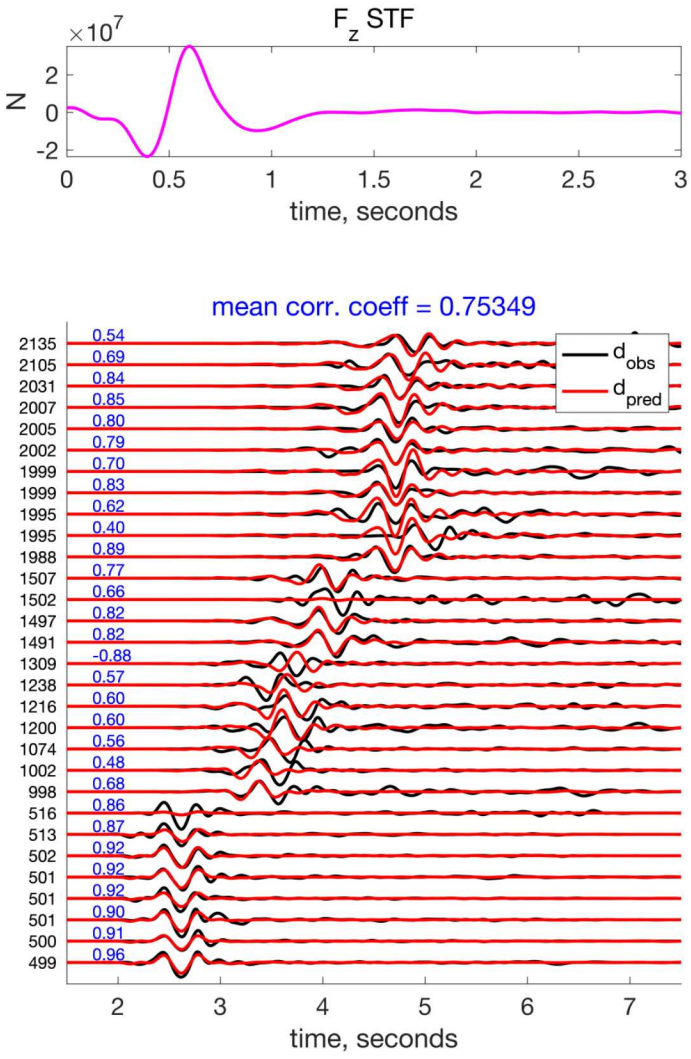


**Figure 3-2. Same as Figure 3.1, but assuming the source model consists only of a vertically oriented force applied at the Earth's surface.**

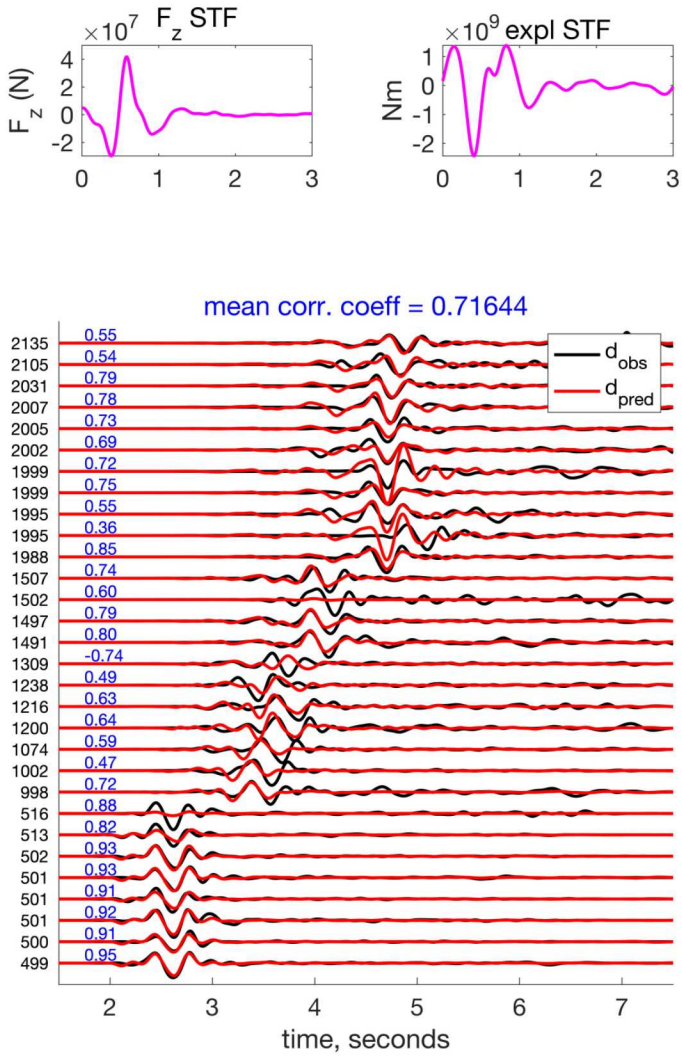


**Figure 3-3. Same as Figure 3.1, but assuming the source model consists of both a buried, isotropic explosion and a vertically oriented force applied at the Earth's surface.**

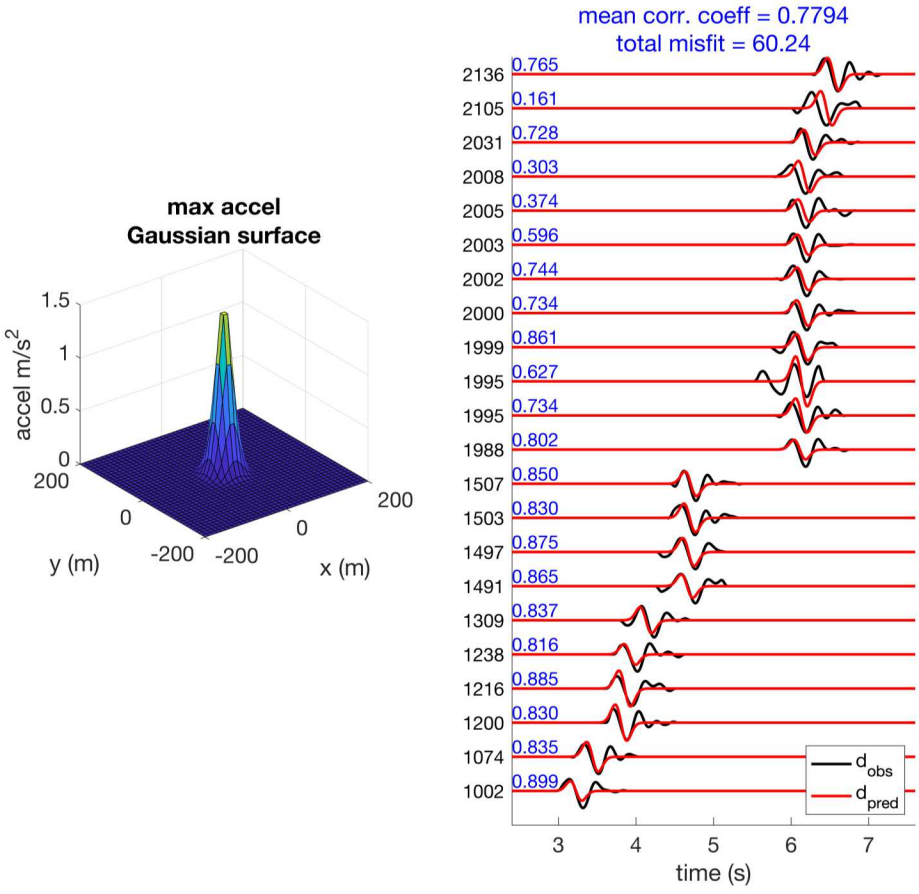


**Figure 3-4. The estimated acceleration surface, assuming the two-dimensional Gaussian model, using the RI-inversion scheme. The panel on the left shows the estimated acceleration surface at the time corresponding to it's maximum amplitude. The panel on the right is similar to that shown in Figure 3.1**

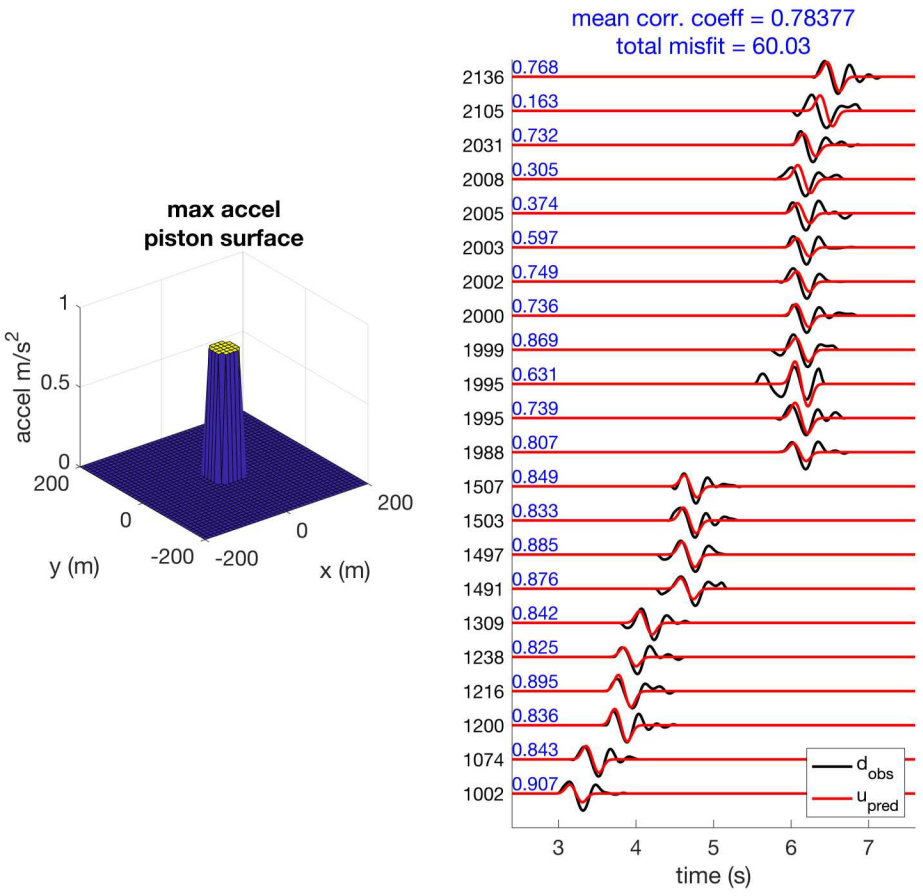


**Figure 3-5. Similar to Figure 3.2, but assuming a piston spall model.**

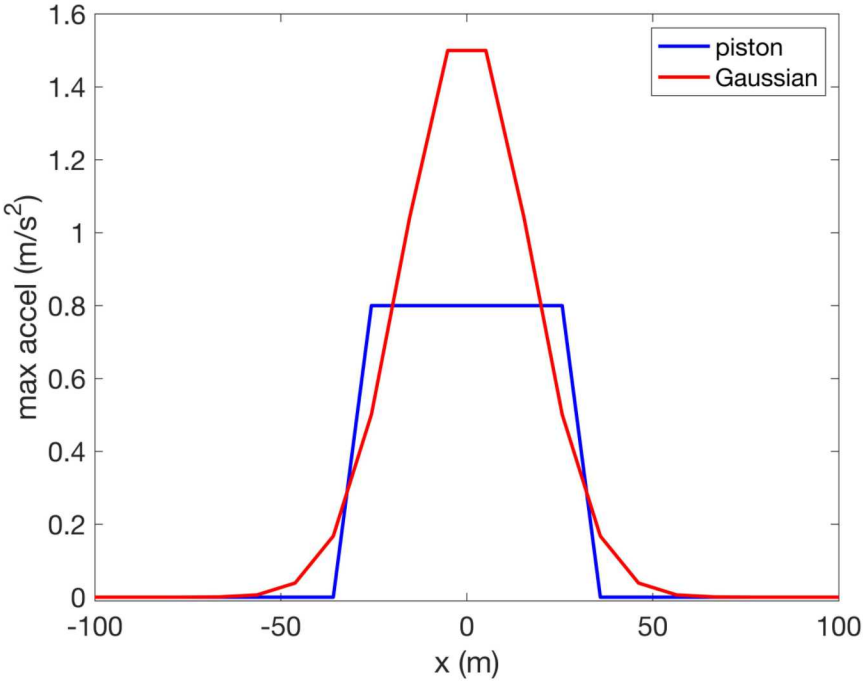


**Figure 3-6. Cross sections through the estimated maximum acceleration surfaces estimated for both model types. Note that the area under each of the curves, and hence the volume under the estimated acceleration surfaces shown in Figures 3.4 and 3.5, are similar.**

# 4. DISCUSSION AND CONCLUSIONS

This report presents the results of analyzing a portion of the SPE Phase II, Dry Alluvium Geology (DAG) infrasound data. The infrasound data were generated by a series of four controlled, underground chemical explosions, each of which had a different yield and depth. However, because of the experimental geometry and the size/depth of the explosions, the instruments deployed as part of this experiment were only able to record a clear source-generated infrasound signal for the fourth DAG explosion.

We used two inversion schemes to analyze the data. For the first method, termed the STF-inversion, we used a similar inversion scheme to that used to analyze the SPE Phase I infrasound data. The STF-inversion is a linear inversion method that is designed to estimate the source time functions of a generalized seismoacoustic source. The forward model is based on an assumed point source, linear wave propagation, and a linear model that predicts the observed data. The second method, termed the RI-inversion, based on previous work where the Rayleigh inversion is used to model the data. The RI-inversion is based on the Rayleigh integral, which predicts that the acoustic wavefield based solely on the vertical acceleration time history of a finite-area surface and the speed of sound in air.

Using the STF-inversion, we inverted the data under three separate source model assumptions: a purely isotropic buried explosion, a single time-variable vertically-oriented force applied to the Earth's surface, and a dual-source model consisting of both the explosion and vertical force. The results of the STF-inversion show that the data is best fit when the source model is approximated by a single vertically oriented vector force, applied to the Earth's surface directly above the buried explosion. However, data fit is almost as good using the other two source models, based on computed misfit parameters. In all cases, the data were fit quite well. Furthermore, the approximate magnitude of the maximum amplitude of the estimated source time functions is similar for each respective source type, regardless of the source model used. This is direct contrast to the results we obtained when inverting the SPE-Phase 1 infrasound data, where we determined that the data is best described as being generated by the surface spall (which we also estimated as a single vertically oriented force). This may be due to the SPE inversion not modeling the explosive portion of the data, whereas the DAG inversion is. For the DAG-4 data, it's likely that the majority of the infrasound is also generated by the surface spall, however, it appears that the isotropic explosion source is also a large contributor to the observed data. This conclusion is based on the stability of the estimated explosion source in the inversions.

To invert the data using the RI-inversion, we must assume an acceleration time history and a functional form for the acceleration surface. Recall that the acceleration surface is designed to approximate the spall. The inversion then attempts to fit the data by finding the amplitude of the acceleration time history and the size parameters of the assumed spall model. For the acceleration

time history, we used a first-derivative Gaussian (1-6 Hz passband), which we found closely resembles the observed data. Note that we used this acceleration time history for both inversions. We inverted the data twice, each time using a different surface acceleration model. For the first case, we assumed that the spall surface could be approximated by a two-dimensional Gaussian, which is parameterized by its half widths in the $x$ and $y$ directions. For the second case, we approximated the spall surface as a piston, where the size is described by the radius $r_0$.

Observations of digital acoustic sensing data (not presented here) suggest that the spall surface was Gaussian-shaped. However, using our RI-inversion we were able to fit the data equally well using both a Gaussian and piston spall model. The estimated Gaussian spall surface was narrower and almost twice the amplitude compared to the estimated piston spall model. However, the volume under each estimated source model were similar, suggesting that for this model geometry the amount of material that is spalled may be more important than that details of (similarly shaped) spall surfaces. Being able to fit the data approximately equally well with these two spall model suggests a fundamental ambiguity with this method. This is perhaps the limitation of our RI-inversion approach in that the inversion will not estimate the functional form of the spall. However, the point of our RI-inversion was to develop a computationally fast method that could fit the data to a very simple model. Adding the capability of estimating the functional form of the spall surface will likely improve the fit-to-data, but it will necessarily add mathematical and computation costs. Rather, the RI-inversion is perhaps more appropriate for a quick, "first-order" estimation of a spall surface that only takes a few seconds to compute. More advanced analysis, the topic of future research, can then be applied later.

Finally, we can compare our RI-inversion results with measured surface accelerations. As part of the instrument deployment during the DAG experiment, an array of surface-deployed accelerometers measured the explosion-induced vertical-component acceleration in the vicinity of SGZ. Although the detailed analysis of the acceleration data will not be addressed in this report, we extracted the value of maximum vertical acceleration to compare to those we estimated using the RI-inversion (Figure 4.1). Examination of the measured maximum acceleration shows that our RI-inversion scheme approximately reproduces the maximum acceleration amplitude, as well as the approximate dimensions. However, based on this figure, our assumption of simple functional models (i.e. a Gaussian and/or a piston) may be overly simplistic. Regardless, the RI-inversion is not designed to find the functional form of the acceleration surface. Rather it's designed to estimate, to the first order, the approximate size and amplitude of the spall surface. In this regard, we argue that the RI-inversion shows promise for future data analysis.

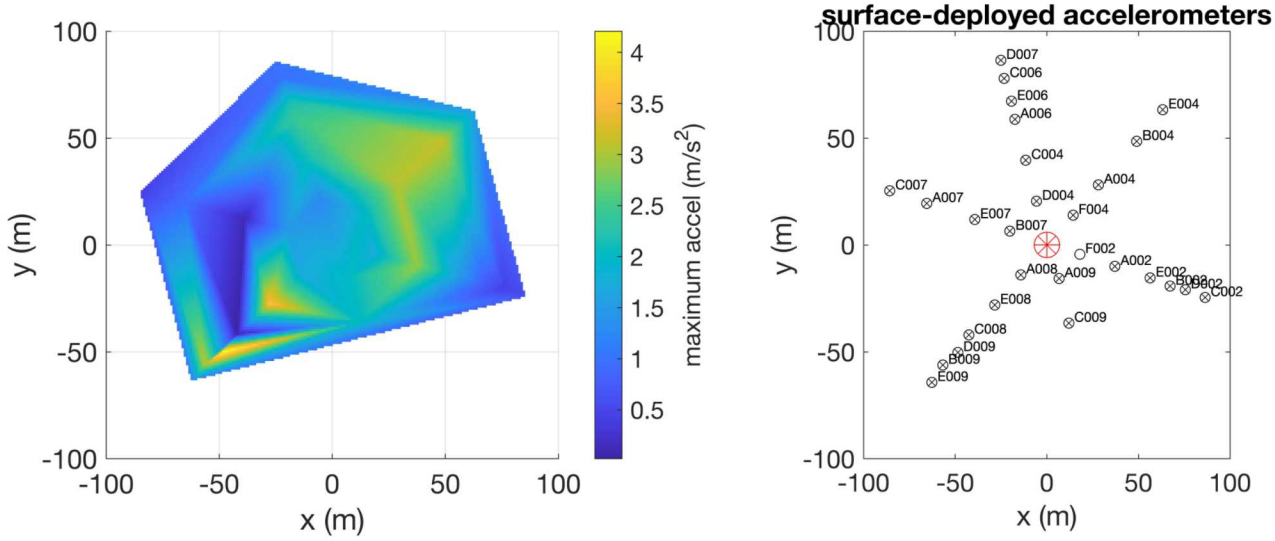


**Figure 4-1. The interpolated maximum acceleration surface (left panel) based on the measured vertical-component acceleration by the accelerometer array deployed around the SGZ (right panel). Note that although the interpolated acceleration surface is more complex than our simple parametric models, the approximate amplitude and spatial extent is similar to our RI-inversion results.**

# 5. REFERENCES


Bannister, J.R. (1979). A program for predicting ground motion induced air pressures, SAND 78-2361, Sandia National Laboratores, Albuquerque, NM.

Kirkup, S.M. (1994). Computational solution of the acoustic field surrounding a baffled panel by the Rayleigh integral method, *Appl. Math. Modeling*, **18**, 403-407.

Mellors, R.J., A. Pitarka, E. Matzel, S. Magana-Zook, D. Knapp, W.R. Walter, T. Chen, C.M. Snelson, R.E. Abbot (2018). The source physics experiment large *N* array, *Seismol. Res. Lett.* **89**(5), doi: 10.1785/0220180072.

Darrh, A., C. Poppeliers, L. Preston (2019). Azimuthally Dependent Seismic-Wave Coherence at the Source Physics Experiment Large-*N* Array, *Bull. Seismol. Soc. Am.*, **109**(5), 1935-1947.

Jones, K.R., R.W. Whitaker, S.J. Arrowsmith (2015). Modelling infrasound signal generation from two underground explosions at the Source Physics Experiment using the Rayleigh integral, *Geophys. J. Int.*, **200**(2), 779-790.

Poppeliers, C., K. A. Aur, L. Preston (2019). The Relative Importance of Assumed Infrasound Source Terms and Effects of Atmospheric Models on the Linear Inversion of Infrasound Time Series at the Source Physics Experiement, *Bull. Seismol. Soc. Am.*, **109**(1), 463-475.

Poppeliers, C., L.B. Wheeler, L. Preston (2020). The Effects of Atmospheric Models on the Estimation of Infrasonic Source Functions at the Source Physics Experiment, *Bull. Seismol. Soc. Am.*, **110**(3), 998-1010.

Prothro, L., H. Huckins-Gang, S. Drellack, D> Reed, M. Townsend, K. Day, T. Kincaid (2016). Three-dimensional seismic-attribute model for Yucca Flat, Nevada National Security Site Fiscal Year 2015 Annual Report, DOE/NV/25946-2758, Las Vegas, Nevada, 189-196.

Snelson, C.M., R.E. Abbott, S.T. Broome, R.J. Mellors, H.J. Patton, A.J. Sussman, M.J. Townsend, W.R. Walter (2013). Chemical explosion experiments to improve nuclear test monitoring, *Eos Trans AGU*, **94**(27), 237-239.

Sweetkind, D. S., R. M. Drake II. (2007). Geologic Characterization of Young Alluvial Basin-Fill Deposits from Drill Hole Data in Yucca Flat, Nye County, Nevada. Open-File Report, 21. http://pubs.er.usgs.gov/publication/ofr20061390.

# DISTRIBUTION

**Hardcopy—Internal**

| Number of Copies | Name | Org. | Mailstop |
|---|---|---|---|
| 1 | Christian Poppeliers | 8861 | 0750 |
| 1 | Leiph Preston | 8861 | 0750 |
| 1 | Kyle Jones | 8861 | 0735 |

**Email—Internal (encrypt for OUO)**

| Name | Org. | Sandia Email Address |
|---|---|---|
| Technical Library | 01177 | libref@sandia.gov |


Sandia National Laboratories is a multimission laboratory managed and operated by National Technology & Engineering Solutions of Sandia LLC, a wholly owned subsidiary of Honeywell International Inc., for the U.S. Department of Energy's National Nuclear Security Administration under contract DE-NA0003525.